Journal of Materials Chemistry C

Accepted Manuscript

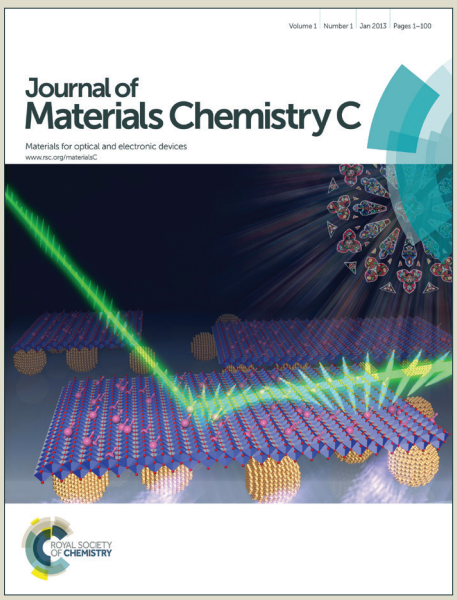

ROYAL SOCIETY OF CHEMISTRY

www.rsc.org/materialsC

Two-step Hydrothermal Synthesis of Sodium Tantalate Nanoparticles with Deep Ultraviolet Sensitivity

Bing Guo,[a,b] Gang Wu,*[,a] Hongzheng Chen*[,a] and Mang Wang [a]

[a] MOE Key Laboratory of Macromolecular Synthesis and Functionalization, State Key Laboratory of Silicon Materials, Cyrus Tang Center for Sensor Materials and Applications, Department of Polymer Science and Engineering, Zhejiang University, Hangzhou, 310027, China

*E-mail addresses: wmang@zju.edu.cn (G. Wu), hzchen@zju.edu.cn (H. Chen)

[b] College of Materials Science and Engineering, China Jiliang University, Hangzhou, 310018, China

Abstract

A convenient two-step hydrothermal method was developed to synthesize water dispersible $NaTaO_3$ nanoparticles. The growth of the $NaTaO_3$ nanoparticles was retarded with the aid of water soluble complex agent in the first step, such as citric acid, bicine, triacetin, and EDTA2Na, which can form complexes with Ta^{5+}. The size of the $NaTaO_3$ nanoparticles ranging from 5 nm to 30 nm could be tuned by adjusting the reaction time and the complex agent as well. The ultraviolet photodetector applying solution processing $NaTaO_3$ film as active layer presented sensitive response to 280 nm deep UV illumination with light to dark current ratio of about 160 times and response time of about 50 ms.

1. Introduction

Alkaline niobate and tantalate semiconductors with a perovskite structure are important function materials having potentials in wide fields because of their various properties like piezoelectric,[1] luminescent,[2-4] photocatalytic,[5-10] pyroelectric,[11] dielectric,[12] ferroelectric[13] and electro-optic[14] properties. The advantage of large surface area for the nanoparticles can help to improve the surface electronic process such as gain/loss and injection/extraction of

the electrons. Conventional methods for synthesizing tantalate and niobate powders are solid state based reaction, which requires long time of heating above 800°C.[6,14] The high temperature treatment results in the large grain size of about 1-2μm. Sol-gel methods can decrease the reaction temperature to 600-700 °C and the grain size to dozens of nanometers.[3, 15-17] But the aggregation of the particles can hardly be avoided. Hydrothermal method manipulated at moderate temperature can be used to synthesize $NaTaO_3$ and $NaNbO_3$ particles with highly crystallinity and low aggregation.[10, 18-22] Li et al. applied a one-step hydrothermal method to synthesize $NaTaO_3$ by using Ta_2O_5 and NaOH as starting materials.[23] Ji et al. adopted Nb foil and low-concentration NaOH solution with the presence of H_2O_2 to prepare $NaNbO_3$ microcubes.[1] Ikeda et al. prepared $A_2Ta_2O_6$ and $A_2Nb_2O_6$ (A = Na, K) by using tantalum or niobium alkoxide as precursor.[24] Most of these reported products have particle size from a few tens of nanometers to micron scale.[25] He et al. reported the preparation of $NaTaO_3$ nanocubes with the edge length of about 5 nm by using $Ta(OC_4H_9)_5$ and NaOH as precursor,[26] the $NaTaO_3$ nanocubes tend to aggregation. The expensive precursor, $Ta(OC_4H_9)_5$, is moisture sensitive and need the protection of inert atmosphere. To the best of our knowledge, the study about the preparation of $NaTaO_3$ nanoparticles ($NaTaO_3$ NPs) with good dispersion stability is still rare.

In this study, we developed a convenient two-step hydrothermal process to prepare water dispersible $NaTaO_3$ NPs. The starting material is cheap and the whole process can be handled in ambient atmosphere. The obtained monoclinic-phase $NaTaO_3$ NPs have good dispersion stability in water. The solution processed $NaTaO_3$ NPs was used to fabricate UV photodetector and presented sensitive response to 280nm UV light.

2. Experimental section

Synthesis of Sodium Tantalate Nanoparticles

All chemicals were of analytical grade and used without further purification. The typical synthetic process could be divided into two steps. The first step was the preparation of the precursor. 7mL ethanol solution of $TaCl_5$ (0.2M) was mixed with 6mL citric acid monohydrate aqueous solution (0.61M) under stirring. 7mL NaOH aqueous solution (0.47M) was added dropwise to above mixture to adjust the pH value. The final solution (pH = 1.5) was transferred into a Teflon-lined autoclave with a capacity of 30mL. The autoclave was sealed and heated at 200^{o}C for 12h, cooled to room temperature in air. The precursor was white gelatinous products which used in the next step after centrifugation, washed and dried in air at 80^{o}C. In the second step, 0.324g precursor, 18mL deionized water, 1.02g NaOH and 6mL glycerol were mixed and added into a Teflon-lined autoclave and heated at 200^{o}C for 4h, cooled to room temperature in air. The obtained $NaTaO_3$ NPs were centrifuged, washed with deionized water twice and dispersed in water to form uniform suspension.

Characterization of $NaTaO_3$ Nanoparticles

The crystallinity of as-prepared sample was examined by a RIGAKU D/MAX 2550/PC X-ray diffraction (XRD) with a Cu Kα radiation source. The morphology was examined by a Hitachi S-4800 field emission scanning electron microscopy (SEM) and a JEOL 2100 transmission electron microscopy (TEM). FTIR spectrum (KBr pellets) was carried out by Bruker Vector 22 Fourier Transform Infrared Spectrometer. X-ray photoelectron spectroscopy (XPS) was performed with a ESCALAB 250Xi

spectrometer. The thermogravimetric analysis (TGA) was examined by TGA Q50 analysis (50 to 800°C, 10°C /min, under nitrogen gas flow). The surface areas of $NaTaO_3$ were evaluated by Tristar II 3020 specific area and porosity analyzer using the method of Brunauer-Emmett-Teller (BET). The optical property of $NaTaO_3$ was tested on a Shimadzu UV-2450 ultraviolet-visible spectrophotometer. Cyclic voltammetry (CV) measurement was conducted with a CHI 660C electrochemical workstation at room temperature with a scan rate of 50mV/s. Film of $NaTaO_3$ was prepared by dropping nanoparticles suspension on the platinum disk electrode. The measuring solution consisted of acetonitrile and 0.1M tetrabutylammonium hexafluorophosphate ($TBAPF_6$, Merck), platinum wire used as counter electrodes, saturated calomel electrode as reference electrode, platinum disk as working electrode.

Device Fabrication and Characterization

The device was fabricated on ITO glass substrates initially coated with a thin layer of PEDOT:PSS (40nm). 80nm active layer of $NaTaO_3$ film was prepared by spin-coating. Finally semitransparent aluminum electrode (10nm) was vacuum evaporated on the $NaTaO_3$ film. To ensure the dispensability of $NaTaO_3$ NPs in chloroform, surface modification of the as-prepared $NaTaO_3$ NPs was performed as follows. 20 ml alcohol as flocculant was added to 15 ml $NaTaO_3$ aqueous suspension. The precipitate was redispersed in hexanoic acid at 105 °C and stirred for 2h. Methanol was added afterwards to precipitate the particles, followed by centrifugation. Then 5ml chloroform and 10ml methanol were added at 90 °C to precipitate the $NaTaO_3$ NPs again. After centrifugation, particles were finally dispersed into chloroform

at a concentration of about 10mg/ml. The current-voltage (I-V) characteristic of the device was measured with an Agilent 4255C Semiconductor Parameter Analyzer both in the dark and under excitation of 280nm LED light source.

3. Results and discussion

Charateristics of Precursor

The SEM image of the as-prepared precursor, friable aggregation-like material, was shown in Figure 1 (a). The XPS spectra shown in Figure 1 (b) indicates that only Ta, O, C element can be detected in the precursor. The XRD pattern of the precursor shown in Figure 1 (c) presents some characteristics of the monoclinic Ta_2O_5 (JCPDS cards 70-4775). It is suggested that the Ta^{5+} may partially bonded with O^{2-} in the precursor because of the hydrolysis and possible polycondensation of $TaCl_5$ in the first step hydrothermal reaction. The FTIR spectra of citric acid and precursor were given in Figure 1 (d). The broad peak beyond 3000 cm^{-1} in the curves of precursor can be ascribed to the -OH stretching vibration of citric acid. The C-H stretching vibration (peak at 2977 cm^{-1}) belongs to $-CH_3$ of ethoxide from the hydrolysis of $TaCl_5$. The antisymmetric COO^- stretch (peak at 1645 cm^{-1}) and carboxylate anion (peak at 1385 cm^{-1}) can be observed in the curve of the precursor rather than the C=O stretching vibration (peak at 1750 cm^{-1} and 1704 cm^{-1}) of citric acid, indicating the role of complexing agent for the citric acid. The peaks ranging from 1000 to 500 cm^{-1} can be ascribed to the Ta-O bond stretching vibration. For the precursor, the Ta-O stretching and Ta-O-Ta bridging stretching presents multiple modes (peaks at 881,774,678,624 and 517 cm^{-1}). [12,23] In the process of the first step, the key is to prevent the formation of precipitant in the form of tantalum oxide hydrate, resulted from the rapid hydrolysis of Ta^{5+}. The reaction of $TaCl_5$ with

absolute ethanol was chosen to synthesized $Ta(OEt)_5$ and the produced $Ta(OEt)_5$ will dissolve in the access absolute ethanol. The access absolute ethanol can also decrease the content of water in the system and ensure the mild hydrolysis of Ta^{5+}. Beside the low price, $TaCl_5$ is much less sensitive to moisture than $Ta(OEt)_5$. If relative humidity is lower than 60 %, $TaCl_5$ can be handled in air atmosphere. The mild hydrolysis of $TaCl_5$ in air will not affect the formation of precursor because the corresponding hydrolysate can also form stabilized complex with citric acid. According to the TGA results, the content of Ta^{5+} in the precursor can be calculated to be about 72% in weight. Thus, the possible structure of the precursor can be speculated, as shown in Figure 2. Parts of Ta^{5+} reacted with ethanol and citric acid during the process of mild hydrolysis of $TaCl_5$. Some O^{2-} in Ta-O network was substituted by $-OC_2H_5$ and citrate, which not only prevents the formation of precipitant in the form of tantalum oxide hydrate, but also restricts the growth of the nanoparticles.

Figure 1.

Figure 2.

Structure and Morphology of the $NaTaO_3$ NPs

Figure 3 (a) gave the XRD pattern of the as-prepared $NaTaO_3$ NPs. The representative peaks of (100), (011), (111), (200), (210) and (121) can be readily indexed as pure monoclinic phase perovskite $NaTaO_3$, corresponding to the reported date of JCPDS cards (74-2477, with a = 3.889Å, b = 3.885 Å and c = 3.889 Å, $\alpha = \gamma = 90^o$ and $\beta = 90.367^o$). The bond angle of this Ta-O-Ta is 180^o, benefits the separation of photoelectron and hole.[4] According to the Scherrer equation, the average size of the $NaTaO_3$ NPs can be calculated to be 8.3 nm.

The morphology of the as-prepared $NaTaO_3$ NPs was given in Figure 3 (b). The particles size estimated from the TEM image (Figure 3 (c)) is about 5-10 nm, matching up with the result calculated from XRD pattern. Because of the steric effect of the solvent alkyl chain in citric acid, good dispersion can be detected in the inset of Figure 3 (c). Figure 3 (d) showed the HRTEM image of as-prepared $NaTaO_3$ NPs. The lattice fringes are visible, illustrating that the NPs are well crystallized. A lattice spacing of 0.385 nm obtained from the HRTEM corresponds to the (100) plane of the monoclinic phase of $NaTaO_3$.

The FTIR spectrum of $NaTaO_3$ NPs shown in Figure 4 (a) presents characteristic strong peak, ranging from 500 to 900 cm^{-1}, of the Ta-O stretching vibration, indicating the formation of the crystalline structure. Besides, the -OH stretching vibration (beyond 3000 cm^{-1}) from citrate, the C-H stretching vibration respectively from the $-CH_2$ of glycerol (peak at 2928 cm^{-1}) and citrate (peak at 2843 cm^{-1}), and the COO^- stretch vibration (peak at 1645 cm^{-1}) can also be detected. It is suggested that the surface of $NaTaO_3$ NPs was capped with citric acid and glycerol ligand. Figure 4 (b) gave the XPS spectra of as-prepared $NaTaO_3$ NPs. In the high-resolution spectra of Figure 4 (c) and Figure 4 (d), the peaks with the binding energy of 27.0 eV and 25.1 eV could be ascribed to Ta($4f_{7/2}$) and Ta($4f_{5/2}$) of Ta^{5+} and the peak at 529.12 eV could be assigned to O1s of $NaTaO_3$.[27, 28]

Figure 3.

Figure 4.

The growth of the $NaTaO_3$ NPs is so slow that we can obtain particles with various sizes by using different time of the second-step reaction. As shown in the TEM images (Figure 5), the size of the $NaTaO_3$ NPs increased with the increasing reaction time from 2 to 12 hours.

From the XRD patterns of the $NaTaO_3$ NPs with different reaction time (Figure 6), the broadening of the (100) diffraction peak with the shortened reaction time can be detected. The particle size was calculated to be about 5.8, 8.3, 11.0, 12.6 nm for 2, 4, 8, 12 hours reaction, respectively. Commonly, the growth of the $NaTaO_3$ NPs under hydrothermal condition is very fast and hard to control, that is why most of $NaTaO_3$ particle size is about hundred nanometers or even larger. The slow growth of the $NaTaO_3$ NPs in this study can be ascribed to the citrate in precursor which hindered the combinations of Ta^{5+} with OH^- and Na^+ by bonding to the Ta^{5+} surfaces and enwrapping the Ta^{5+} ions inside. Besides, glycerol, used in the second step, can employed as size-controlling agent to restrict the growth of the nanoparticles.[29-31]

The BET surface area of these particles was measured and summarized in Table 1. The submicron $NaTaO_3$ particles, 200-300nm in size, were synthesized by traditional one-step hydrothermal method for comparison.[23] Generally, the BET surface area increases with the decreasing particle size. Because of the biggest size, the BET surface area of the submicron paritcles, 4.09 m^2/g, was the smallest among the five samples. The smallest particles, 5.8 nm in size, have the largest BET surface area, 119.36 m^2/g. For the $NaTaO_3$ NPs with size of 8.3, 11.0, 12.6 nm, the BET surface area, about 70 m^2/g, was almost particle-size independent, which could be ascribed to the aggregation of the $NaTaO_3$ NPs in powder state. The method established here paves a new way to control the growth of the nano tantalate and gives a method to prepared $NaTaO_3$ NPs with large surface area.

Table 1.

Figure 5.

Figure 6.

Besides citric acid, we found that other water soluble complexing agents can also be applied to restrict the growth of the $NaTaO_3$ NPs. Here, Bicine, Triacetin, and EDTA2Na were selected to substitute citric acid. The time of second-step reaction fixed at 4 hours. The morphology of the resulting products was given in the TEM images (Figure 7). All of the particles sizes are smaller than 100 nm, in which the size of the Triacetin-based particles is the smallest, about 10-20 nm. The size of the other two particles is a little bigger, about 20-30 nm in diameter. Obviously, the ligand structure can also influence the particle size. In other words, adjusting the structure of the ligand in precursor can also be applied to control the size of $NaTaO_3$ NPs. The effect of ligand structure may be assigned to the different complexing ability of the ligand. During the first-step reaction, because of the strong complexing ability of EDTA2Na and Bicine with Ta^{5+}, gelation was easier to be observed when EDTA2Na and Bicine were used. This phenomenon indicated that the low solubility of the EDTA2Na/Bicine based precursor and the resulting high local concentration of Ta^{5+} in the second step could be expected, which can be considered to be the possible reason why EDTA2Na/Bicine produces $NaTaO_3$ NPs with relatively bigger size.

Figure 7.

Deep UV response of the $NaTaO_3$ film

The UV-vis absorption spectra of the as-prepared $NaTaO_3$ NPs and the spin-coating film were given in Figure 8 (a). It is reported that the absorption onset values of $NaTaO_3$ synthesized by one-step hydrothermal and solid-state methods are 304 and 310nm,

respectively.[23] The absorption onset value of the as-prepared $NaTaO_3$ solution in this study blue shifted to about 290 nm. The band gap (E_g) of the $NaTaO_3$ film was calculated to be 4.13 eV by the formula, $E_g = 1240/\lambda$, in which λ is absorption onset of UV-vis absorption spectrum of the $NaTaO_3$ film (λ = 300 nm).

The energy level of the $NaTaO_3$ NCs (film) was measured by cyclic voltammetry (CV) method. According to the CV curve shown in Figure 8 (b), the E_{red} of $NaTaO_3$ NPs (film) was -0.78 V. The corresponding conduction band level (E_{con}) could be calculated to be -3.62 eV according to the formula, $E_{con} = -(E_{red}+4.4)$ eV. The valence band level (E_{val}) could be calculated to be -7.75 eV, according to the formula, $E_{val}=E_{con}-E_g$.

Figure 8.

The J-V curve of the device in the dark and under 3.6 mW/cm^2 280nm UV light illumination was given in Figure 9 (a). The device structure of ITO/PEDOT:PSS/$NaTaO_3$/Al was shown in the inset. The dark current curve is nonlinear and quasi-symmetrical, indicating the presence of the double Schottky barrier at the interface. Under UV irradiation, the device presents apparently photocurrent response. At 5V reverse bias, the photocurrent is 1.24 mA/cm^2, and the dark current is 7.7×10^{-3} mA/cm^2. The light to dark current ratio is about 160. The photoresponse behavior of the device was characterized by measuring the current as a function of time when the 6mW/cm^2 280nm UV light was periodically turned on and off (Figure 9 (b)). The measurement bias was fixed at reverse bias of 0.2 V. A reproducible response with response time of about 50 ms can be detected, which is comparative to the reported hybrid UV sensor with rapid response.[32-34] It is suggested that the device has promising prospect in the detection of deep UV light.

Figure 9.

4. Conclusions

In this article, water dispersible $NaTaO_3$ NPs have been successfully synthesized by a convenient two-step hydrothermal method. The preparation of the precursor in the first step made a strong bonding between the water soluble complex agent and Ta^{5+} cations, which was helpful for restricting the growth of the $NaTaO_3$ NPs by retarding the combination of Ta^{5+} with OH^- and Na^+. Both of the reaction time and complex regent could be adjusted to influence the size of $NaTaO_3$ NPs ranging from 5 nm to 30nm, roughly. Ultraviolet photodetector using spin-coating film of the $NaTaO_3$ NPs showed sensitive response to deep UV signals. Under 280nm UV illumination, the light to dark current ratio was about 160 times at 5V reverse bias and the response time is about 50 ms.

Acknowledgements

This work was financially supported by the National Natural Science Foundation of China (Grant 51173159, 51373151), the Fundamental Research Funds for the Central Universities of China (2014QNA4037) and Zhejiang Province Natural Science Foundation (No.LR15E030001).

References

1 S. Ji, H. Liu, Y. Sang, W. Liu, G. Yu and Y. Leng, *CrystEngComm*, 2014, **16**, 7598.

2 M. Wiegel, M. H. J. Emond, E. R. Stobbe and G. Blasse, *J. Phys. Chem. Solids*, 1994, **55**, 773-778.

3 Y.-C. Lee, H. Teng, C.-C. Hu and S.-Y. Hu, *Electrochem. Solid-State Lett.*, 2008, **11**, 1.

4 C.-C. Hu, C.-C. Tsai and H. Teng, *J. Am. Ceram. Soc.*, 2009, **92**, 460.

5 H. Kato and A. Kudo, *Catal. Today*, 2003, **78**, 561.

6 H. Kato and A. Kudo, *J. Phys. Chem. B*, 2001, **105**, 4285.

7 A. Kudo and H. Kato, *Chem. Phys. Lett.*, 2000, **331**, 373.

8 J. Wang, S. Su, B. Liu, M. Cao and C. Hu, *Chem. Commun.*, 2013, **49**, 7830.

9 X. Li, Q. Li and L. Wang, *Phys. Chem.y Chem. Phys.*, 2013, **15**, 14282.

10 C. Shifu, J. Lei, T. Wenming and F. Xianliang, *Dalton T.*, 2013, **42**, 10759.

11 P. Combette, L. Nougaret, A. Giani and F. Pascal-delannoy, *J. Cryst. Growth*, 2007, **304**, 90.

12 V. Shanker, S. L. Samal, G. K. Pradhan, C. Narayana and A. K. Ganguli, *Solid State Sci.*, 2009, **11**, 562.

13 S. Zlotnik, P. M. Vilarinho, M. E. V. Costa, J. Agostinho Moreira and A. Almeida, *Cryst. Growth & Des.*, 2010, **10**, 3397.

14 X. Wang, J. Wang, Y. Yu, H. Zhang and R. I. Boughton, *J. Cryst. Growth*, 2006, **293**, 398.

15 C.-C. Hu, Y.-L. Lee and H. Teng, *J. Mater. Chem.*, 2011, **21**, 3824.

16 T. Ishihara, N. S. Baik, N. Ono, H. Nishiguchi and Y. Takita, *J. Photoch. Photobio. A: Chem.*, 2004, **167**, 149.

17 W.-H. Lin, C. Cheng, C.-C. Hu and H. Teng, *Appl. Phys. Lett.*, 2006, **89**, 211904.

18 J. W. Liu, G. Chen, Z. H. Li and Z. G. Zhang, *Int. J. Hydrogen Energ.*, 2007, **32**, 2269.

19 H. Fu, S. Zhang, L. Zhang and Y. Zhu, *Mater. Res. Bull.*, 2008, **43**, 864.

20 X. Li and J. Zang, *Catal. Commun.*, 2011, **12**, 1380.

21 E. Mensur-Alkoy, Y. Ozeren and S. Alkoy, 2013 Joint UFFC and PFM Symposium, 2013, 96.

22 T. Yokoi, J. Sakuma, K. Maeda, K. Domen, T. Tatsumi and J. N. Kondo, *Phys. Chem. Chem. Phys.*, 2011, **13**, 2563.

23 X. Li and J. Zang, *J. Phys. Chem. C*, 2009, **113**, 19411.

24 S. Ikeda, M. Fubuki, Y. K. Takahara and M. Matsumura, *Appl. Catal. A: Gen.*, 2006, **300**, 186.

25 M. Mann, S. Jackson and J. Kolis, *J. Solid State Chem.*, 2010, **183**, 2675.

26 Y. He and Y. Zhu, *Chem. Lett*., 2004, **33**, 900.

27 J. Wang, S. Su, B. Liu, M. Cao and C. Hu, *Chem. Commun*., 2013, **49**, 7830.

28 X. Wu, S. Yin, Q. Dong and T. Sato, *Phys. Chem. Chem. Phys*., 2013, **15**, 20633.

29 Q. Zhang, N. Li, J. Goebl, Z. Lu and Y. Yin, *J. Am. Chem. Soc*., 2011, **133**, 18931

30 L. Zhou, Z. Gu, X. Liu, W. Yin, G. Tian, L. Yan, S. Jin, W. Ren, G. Xing, W. Li, X. Chang, Z. Hu and Y. *Zhao, J. Mater. Chem*., 2012, **22**, 966.

31 D. Steinigeweg and S. Schlucker, *Chem. Commun*., 2012, **48**, 8682.

32 Y. Han, G. Wu, M. Wang and H. Chen, *Polymer*, 2010, **51**, 3736.

33 H.-G. Li, G. Wu, M.-M. Shi, L.-G. Yang, H.-Z. Chen and M. Wang, *Appl. Phys. Lett.*, 2008, **93**, 153309.

34 Y. Han, C. Fan, G. Wu, H.-Z. Chen and M. Wang, *J. Phys.Chem. C*, 2011, **115**, 13438.

Legends to Figures

Figure 1. SEM image (a), XPS spectra (b), XRD pattern (c) of the precursor, FTIR spectrum of citric acid and precursor (d).

Figure 2. Schemetic structure of the precursor.

Figure 3. XRD pattern (a), SEM image (b), SEM image (c), HRTEM image (d) of the as-prepared $NaTaO_3$ NPs. The inset is the suspension of $NaTaO_3$ NPs in water.

Figure 4. FTIR spectra (a), XPS spectra (b) of as-prepared $NaTaO_3$ NPs, high-resolution XPS of Ta 4f (c) and O 1s (d) core level.

Figure 5. TEM images of as-prepared $NaTaO_3$ NPs with different reaction time. 2H (a), 4H (b) , 8H (c), 12H(d).

Figure 6. XRD pattern (a), enlarged (100) plane diffraction peak (b) of as-prepared $NaTaO_3$ NPs with different reaction time.

Figure 7. TEM images of $NaTaO_3$ NPs prepared from Bicine (a), Triacetin (b), EDTA2Na (c).

Figure 8. UV-vis absorption spectra of the $NaTaO_3$ solution and spin-coating film (a), CV curve of the $NaTaO_3$ spin-coating film (b).

Figure 9. J-V curves in the dark and under 3.6mW/cm^2 280 nm UV radiation (a), Transient response curve at -0.2V (b).

Table 1. BET surface area of $NaTaO_3$ particles with different sizes

size (nm)	**BET surface area (m^2/g)**	**preparation methods**	**ref.**
5.8	119.36	Two-step Hydrothermal	This work
8.3	73.39	Two-step Hydrothermal	This work
11.0	70.35	Two-step Hydrothermal	This work
12.6	72.22	Two-step Hydrothermal	This work
200-300	4.09	One-step Hydrothermal	*23*

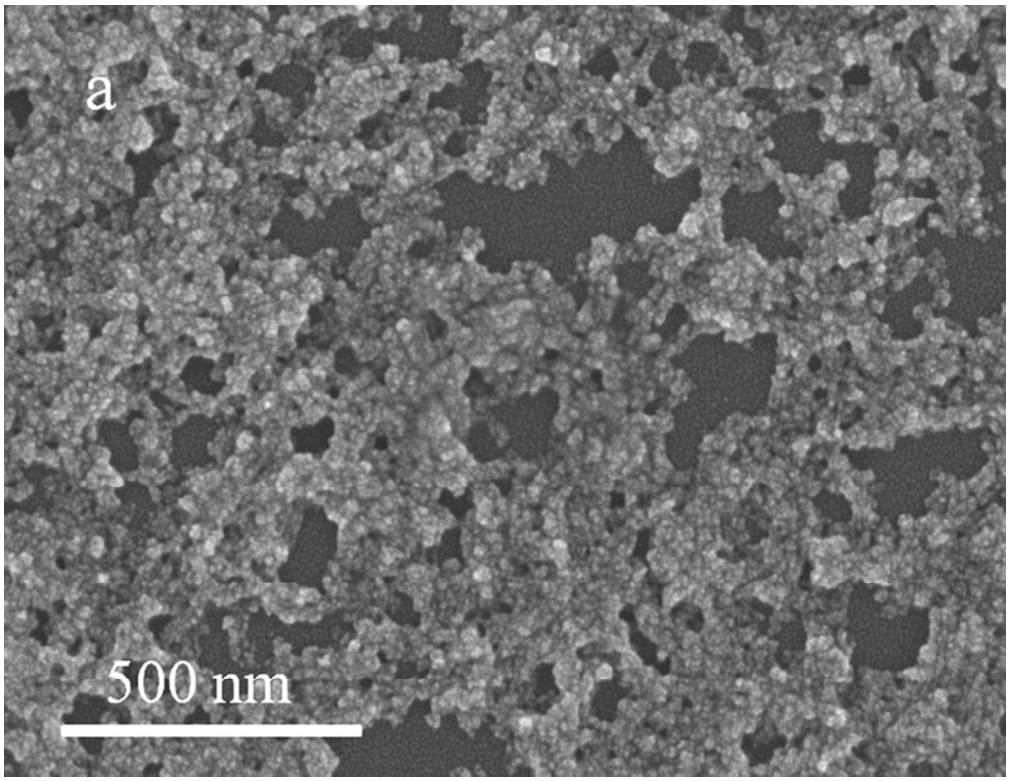

Figure 1. SEM image (a), XPS spectra (b), XRD pattern (c) of the precursor, FTIR spectrum of citric acid and precursor (d).
65x50mm (300 x 300 DPI)

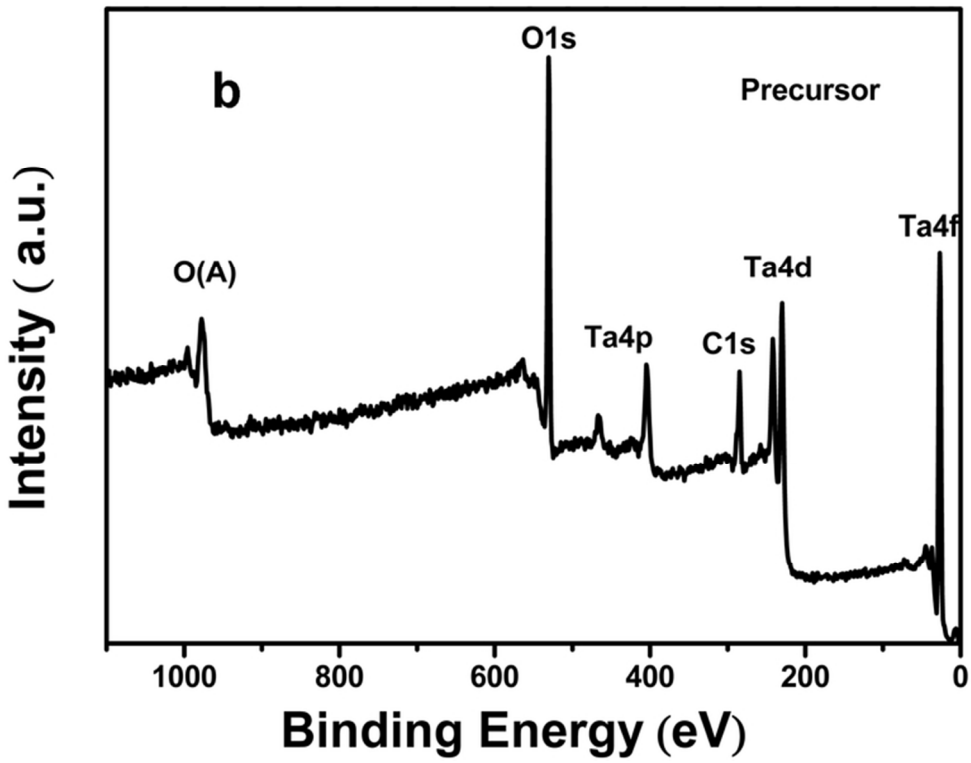

Figure 1. SEM image (a), XPS spectra (b), XRD pattern (c) of the precursor, FTIR spectrum of citric acid and precursor (d).
66x52mm (300 x 300 DPI)

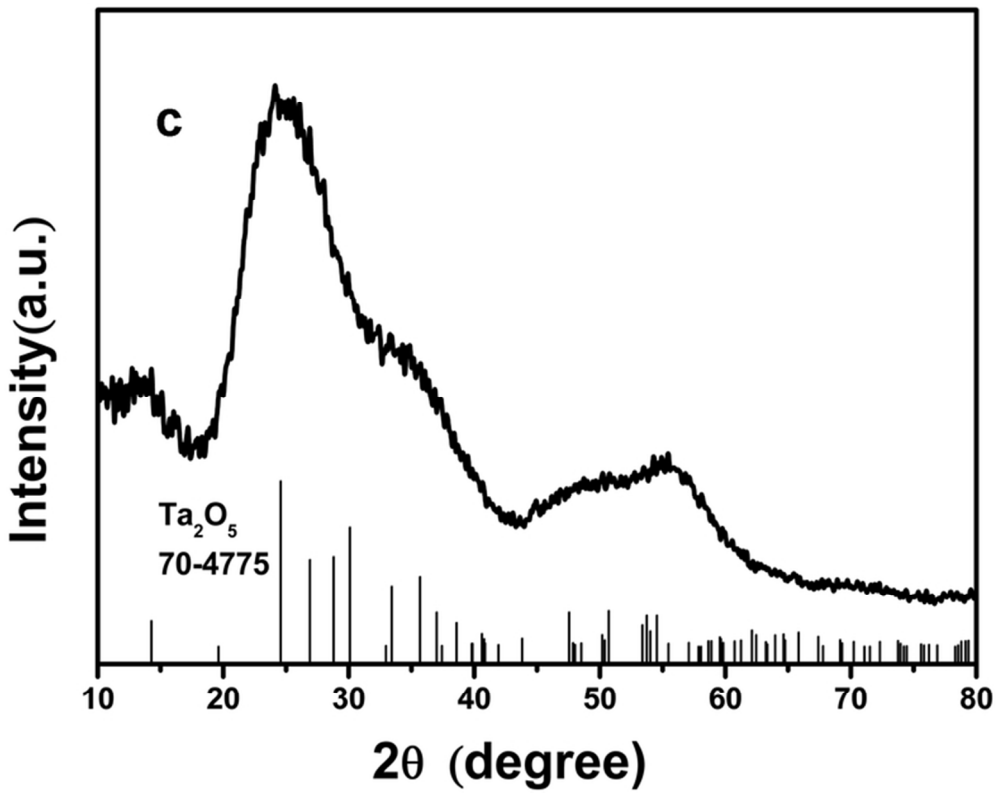

Figure 1. SEM image (a), XPS spectra (b), XRD pattern (c) of the precursor, FTIR spectrum of citric acid and precursor (d).
66x52mm (300 x 300 DPI)

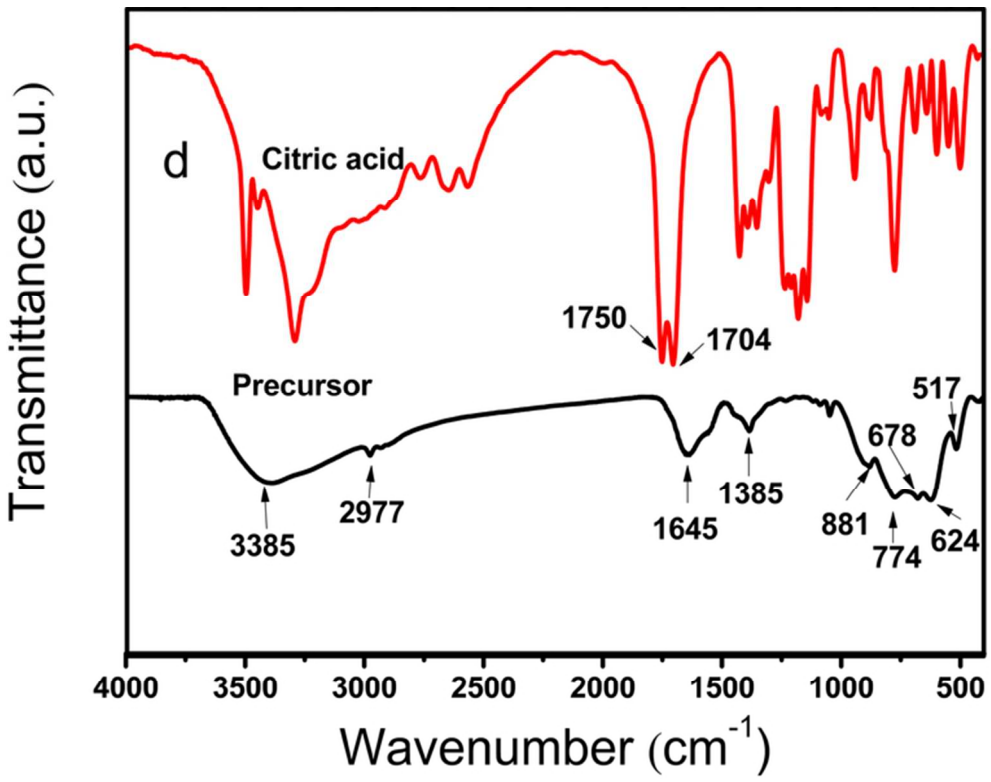

Figure 1. SEM image (a), XPS spectra (b), XRD pattern (c) of the precursor, FTIR spectrum of citric acid and precursor (d).
65x50mm (300 x 300 DPI)

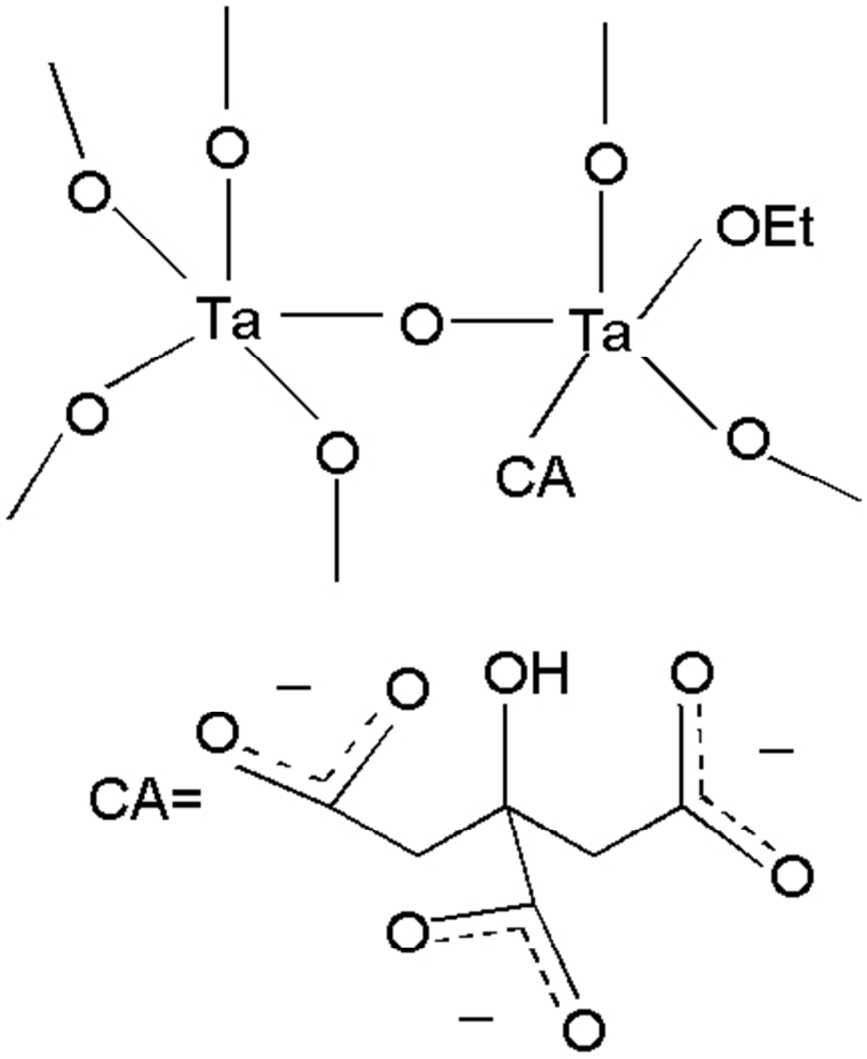

Figure 2. Schemetic structure of the precursor.
36x44mm (300 x 300 DPI)

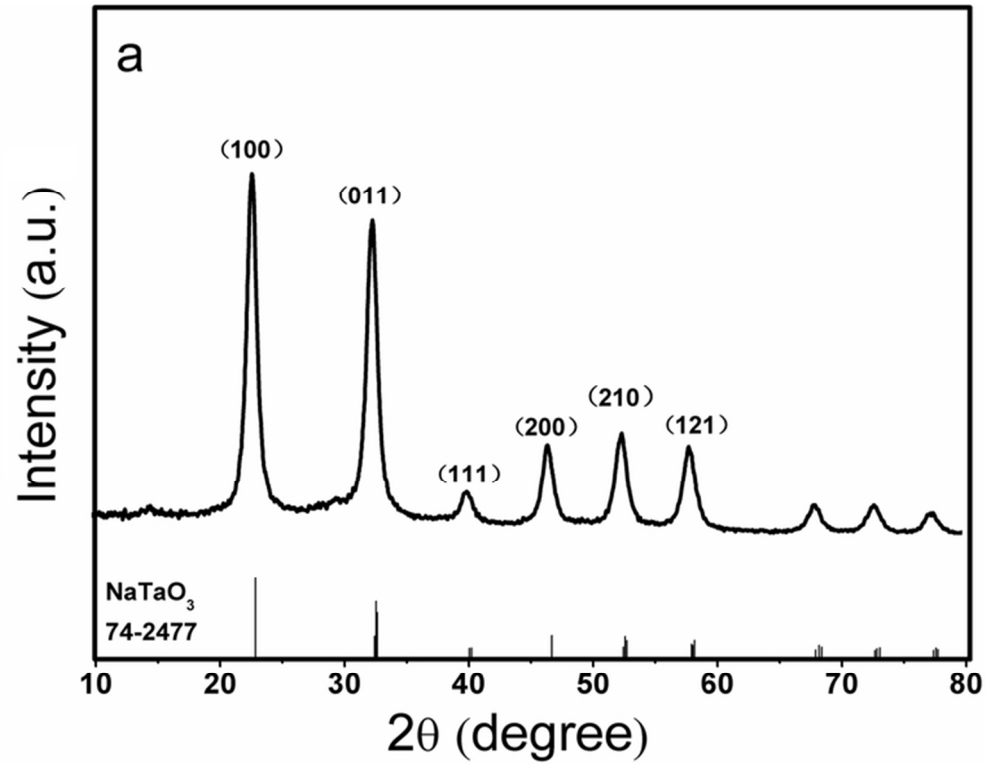

Figure 3. XRD pattern (a), SEM image (b), SEM image (c), HRTEM image (d) of the as-prepared NaTaO3 NPs. The inset is the suspension of NaTaO3 NPs in water.
65x50mm (300 x 300 DPI)

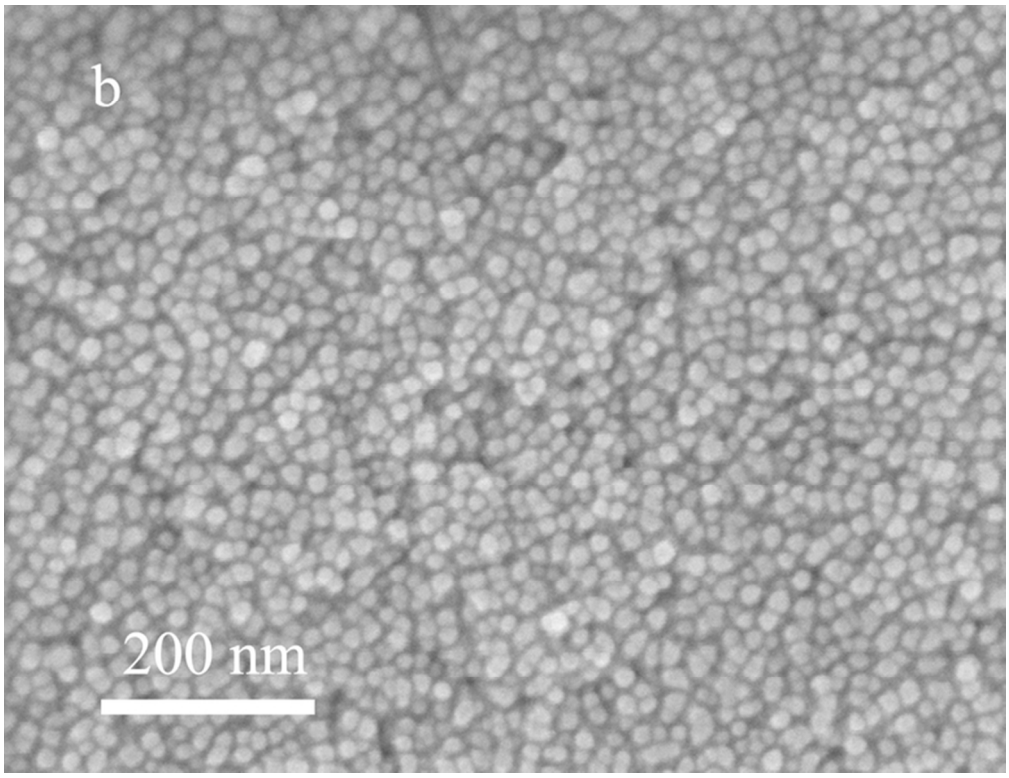

Figure 3. XRD pattern (a), SEM image (b), SEM image (c), HRTEM image (d) of the as-prepared NaTaO3 NPs. The inset is the suspension of NaTaO3 NPs in water.
65x50mm (300 x 300 DPI)

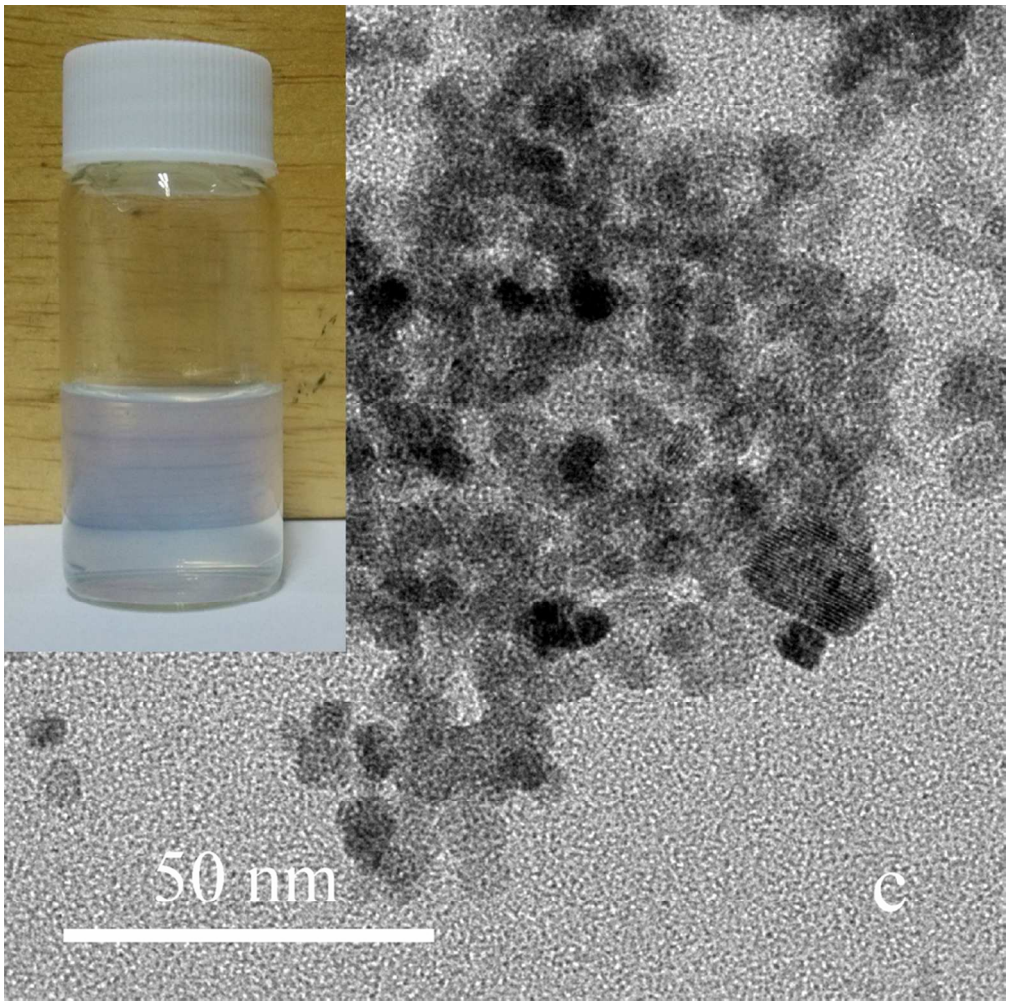

Figure 3. XRD pattern (a), SEM image (b), SEM image (c), HRTEM image (d) of the as-prepared NaTaO3 NPs. The inset is the suspension of NaTaO3 NPs in water.
85x84mm (300 x 300 DPI)

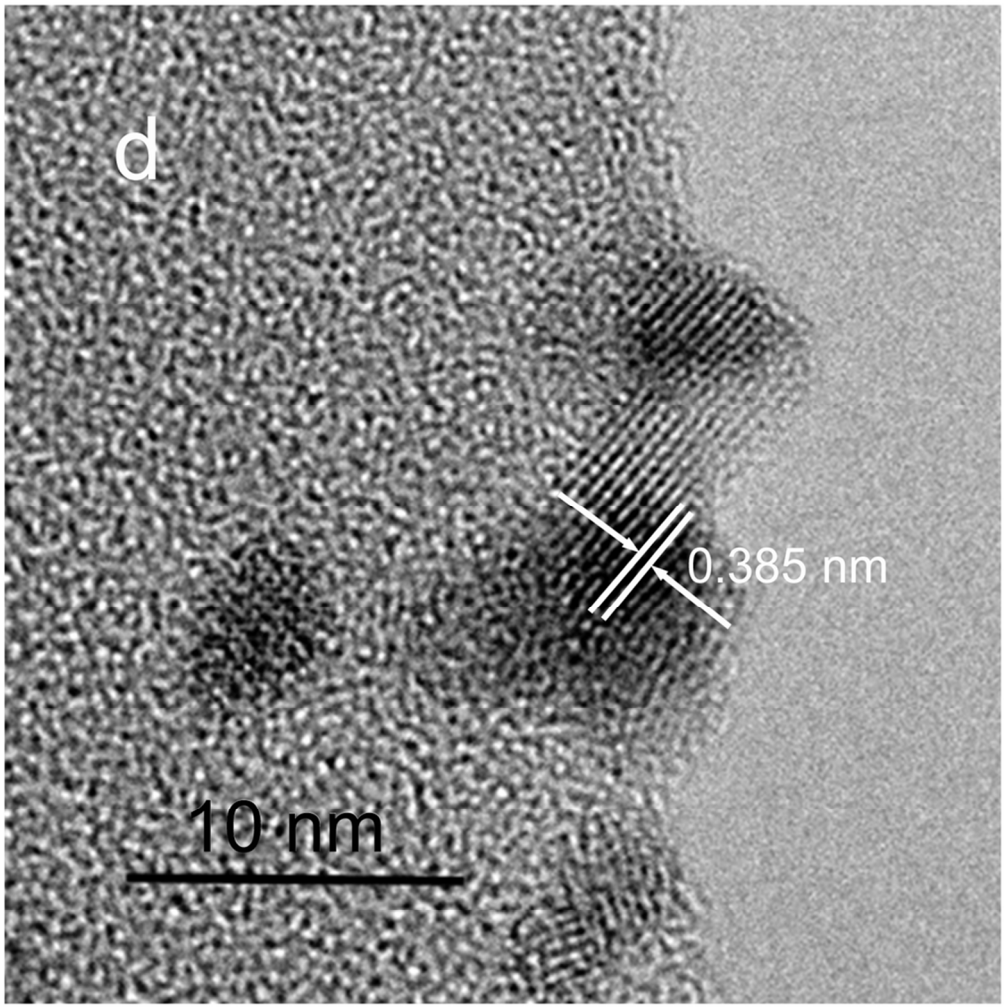

Figure 3. XRD pattern (a), SEM image (b), SEM image (c), HRTEM image (d) of the as-prepared NaTaO3 NPs. The inset is the suspension of NaTaO3 NPs in water.
85x86mm (300 x 300 DPI)

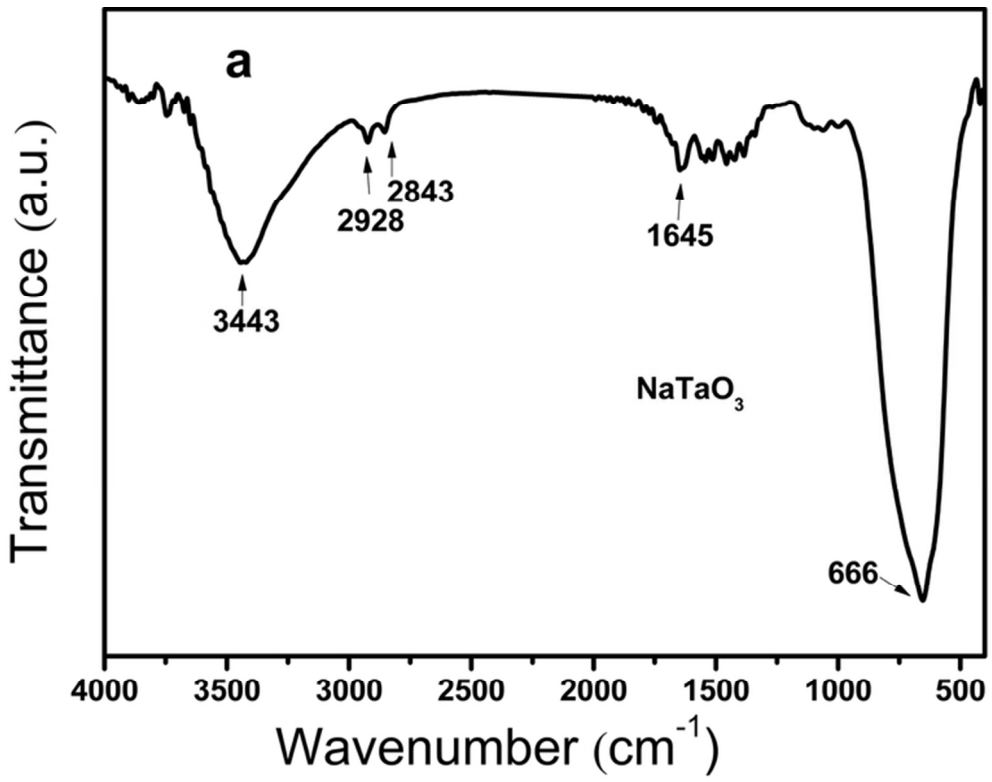

Figure 4. FTIR spectra (a), XPS spectra (b) of as-prepared NaTaO3 NPs, high-resolution XPS of Ta 4f (c) and O 1s (d) core level.
65x50mm (300 x 300 DPI)

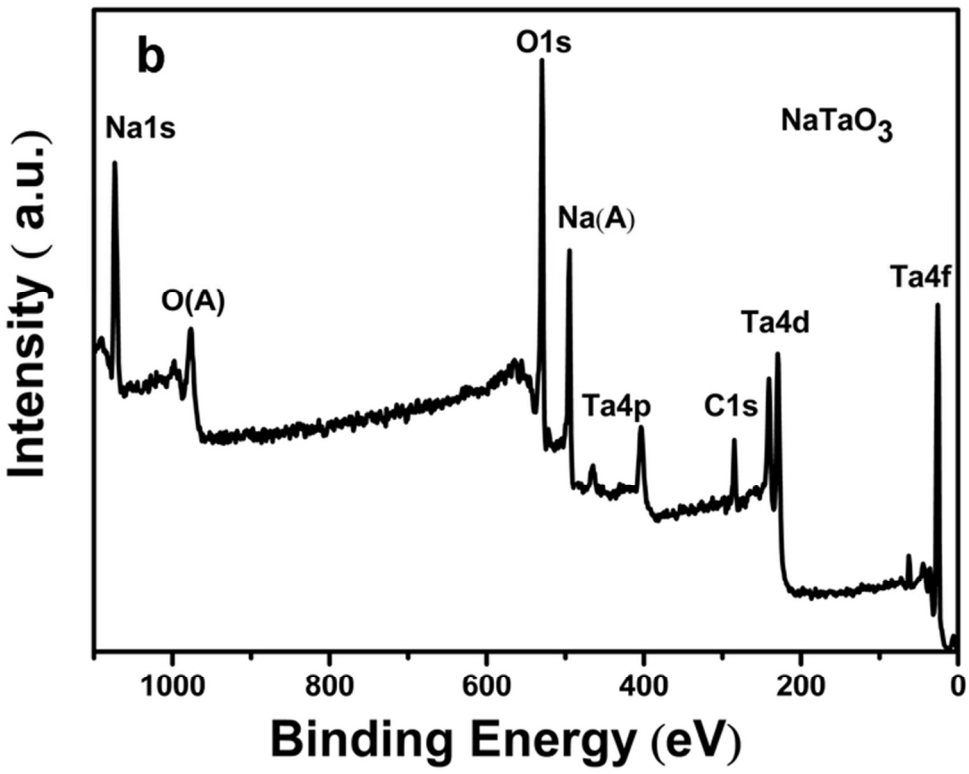

Figure 4. FTIR spectra (a), XPS spectra (b) of as-prepared NaTaO3 NPs, high-resolution XPS of Ta 4f (c) and O 1s (d) core level.
65x50mm (300 x 300 DPI)

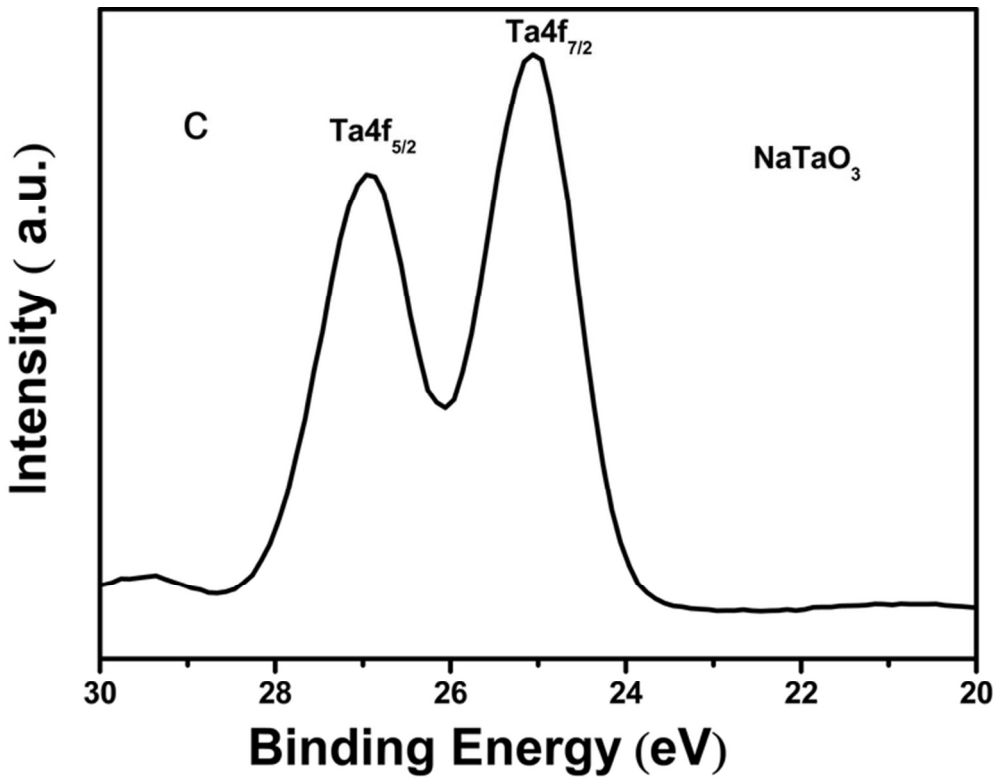

Figure 4. FTIR spectra (a), XPS spectra (b) of as-prepared NaTaO3 NPs, high-resolution XPS of Ta 4f (c) and O 1s (d) core level.
65x50mm (300 x 300 DPI)

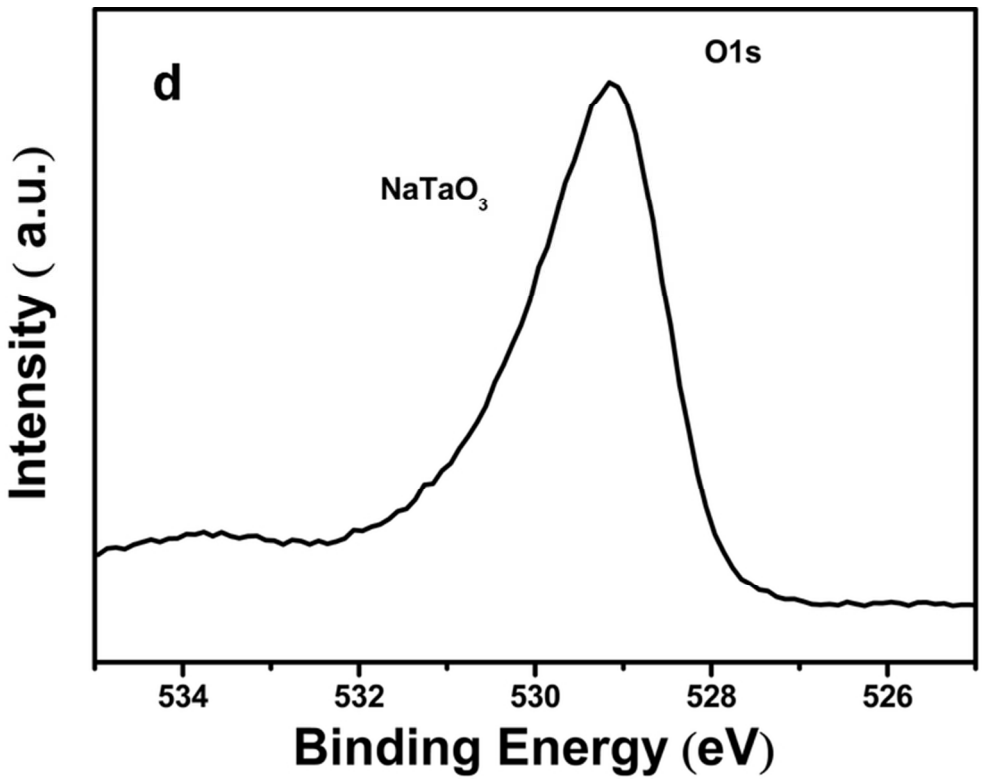

Figure 4. FTIR spectra (a), XPS spectra (b) of as-prepared NaTaO3 NPs, high-resolution XPS of Ta 4f (c) and O 1s (d) core level.
65x50mm (300 x 300 DPI)

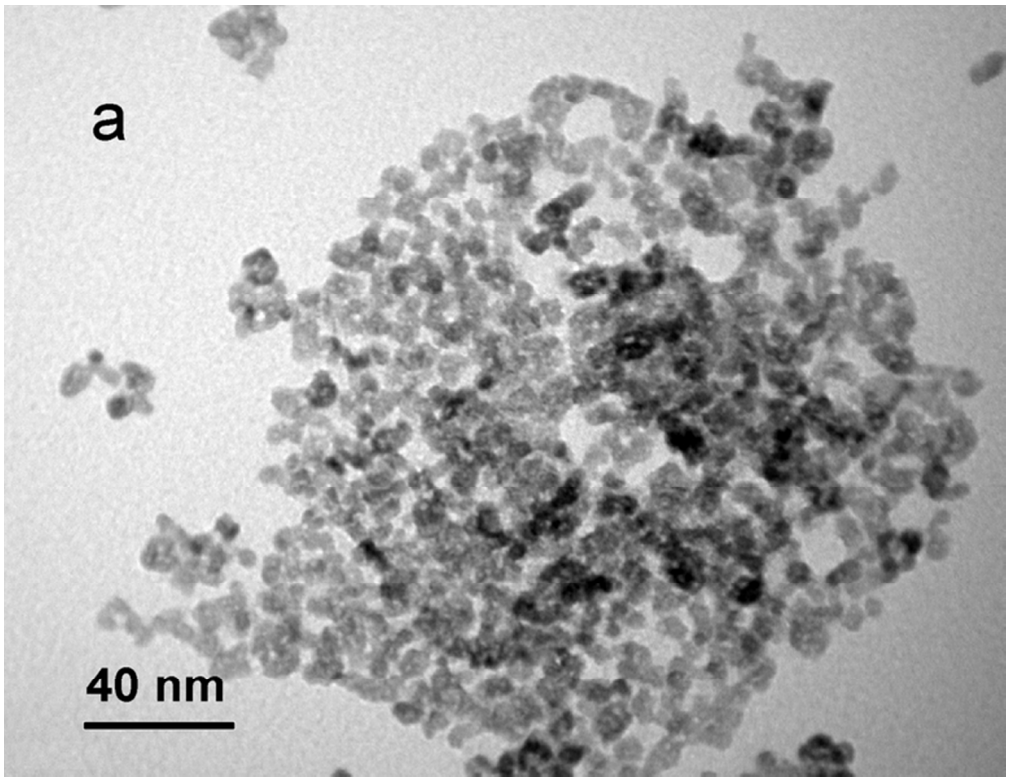

Figure 5. TEM images of as-prepared NaTaO3 NPs with different reaction time. 2H (a), 4H (b) , 8H (c), 12H(d).
65x50mm (300 x 300 DPI)

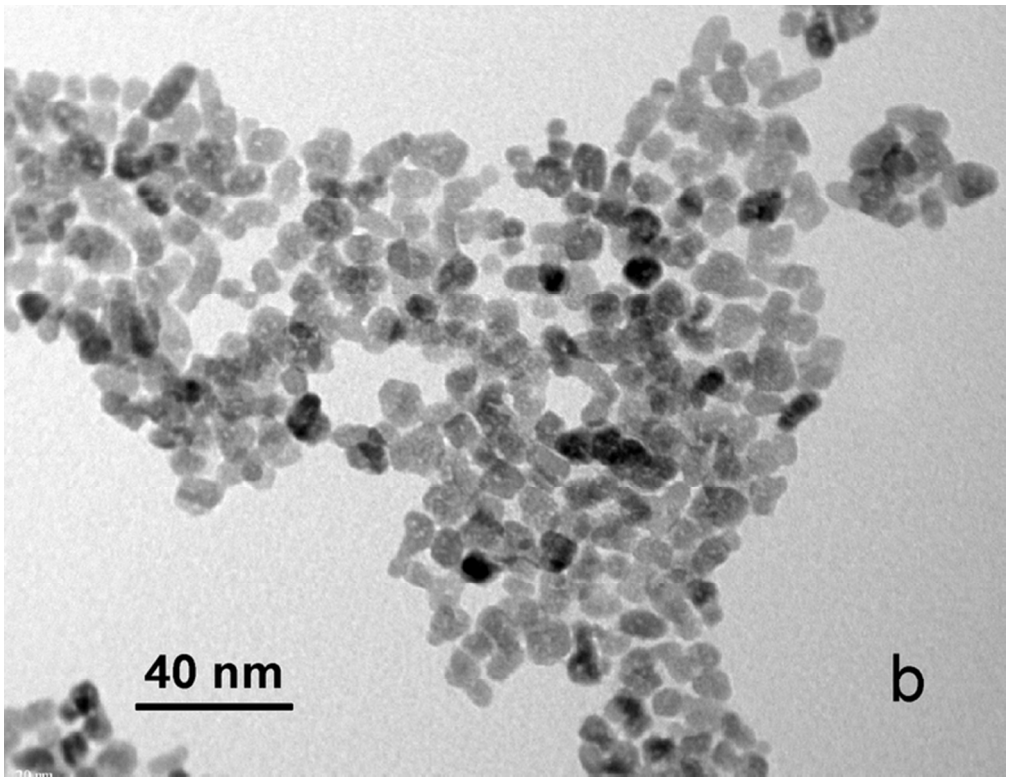

Figure 5. TEM images of as-prepared NaTaO3 NPs with different reaction time. 2H (a), 4H (b) , 8H (c), 12H(d).
65x50mm (300 x 300 DPI)

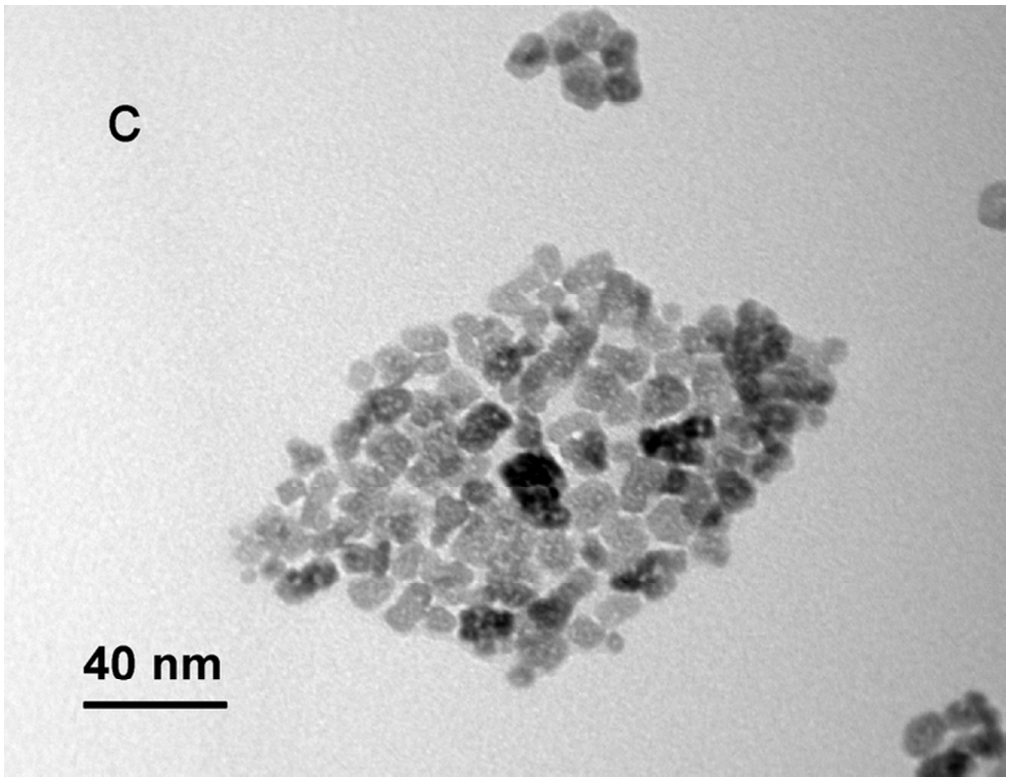

Figure 5. TEM images of as-prepared NaTaO3 NPs with different reaction time. 2H (a), 4H (b) , 8H (c), 12H(d).
65x50mm (300 x 300 DPI)

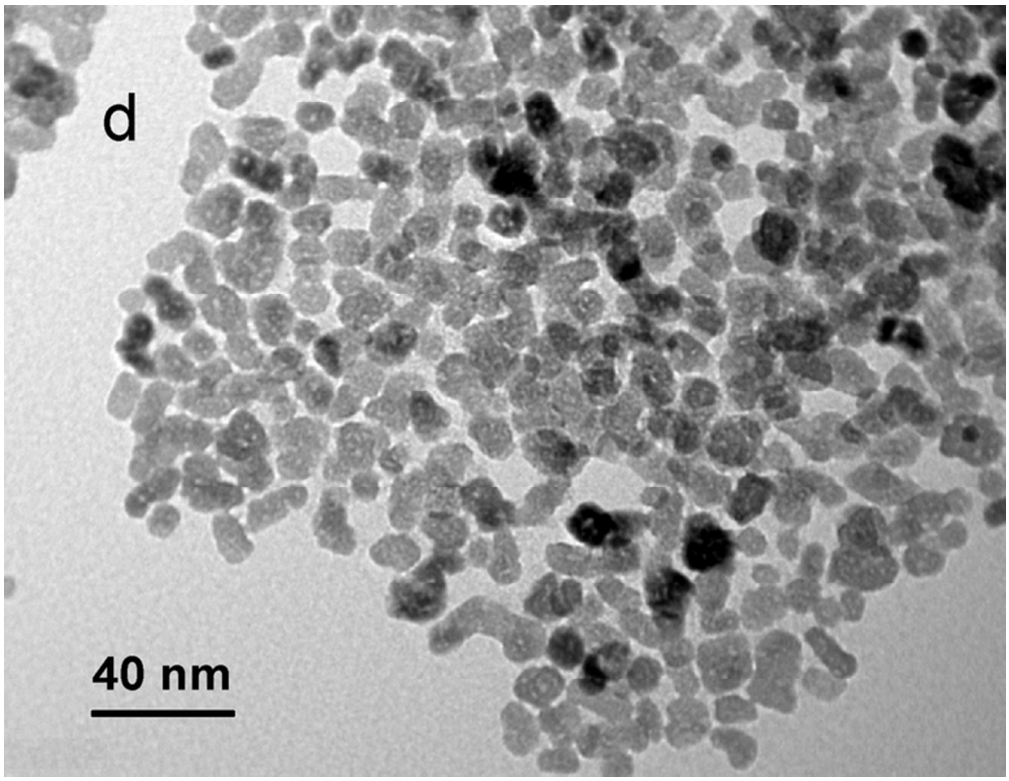

Figure 5. TEM images of as-prepared NaTaO3 NPs with different reaction time. 2H (a), 4H (b) , 8H (c), 12H(d).
65x50mm (300 x 300 DPI)

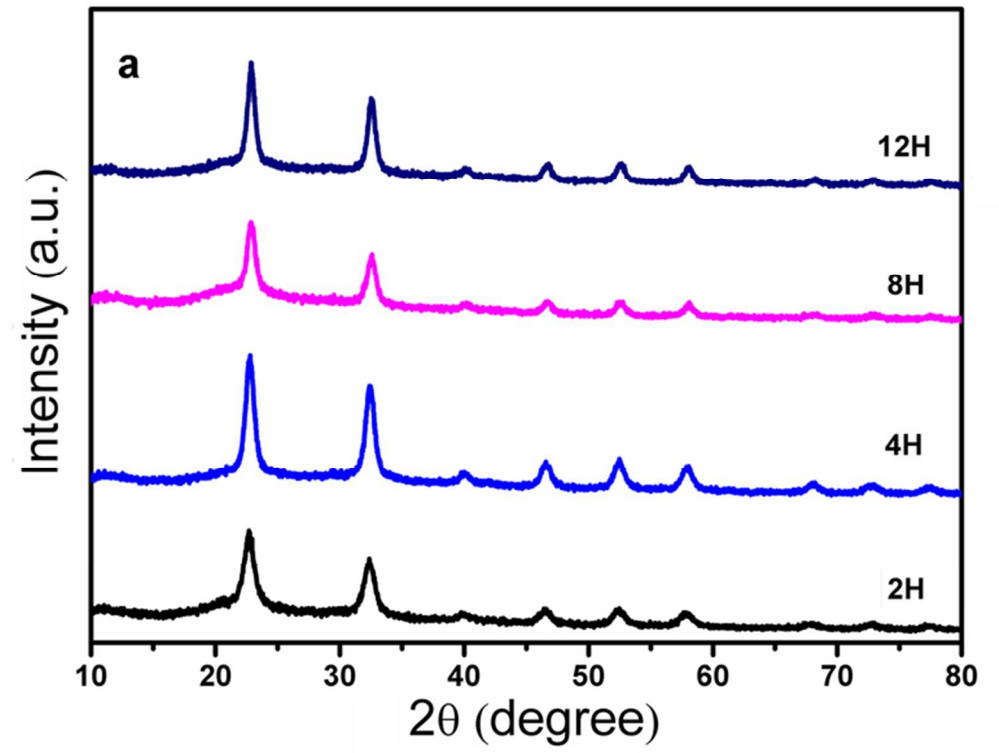

Figure 6. XRD pattern (a), the (100) plane diffraction peak (b) of as-prepared NaTaO3 NPs with different reaction time.
65x50mm (300 x 300 DPI)

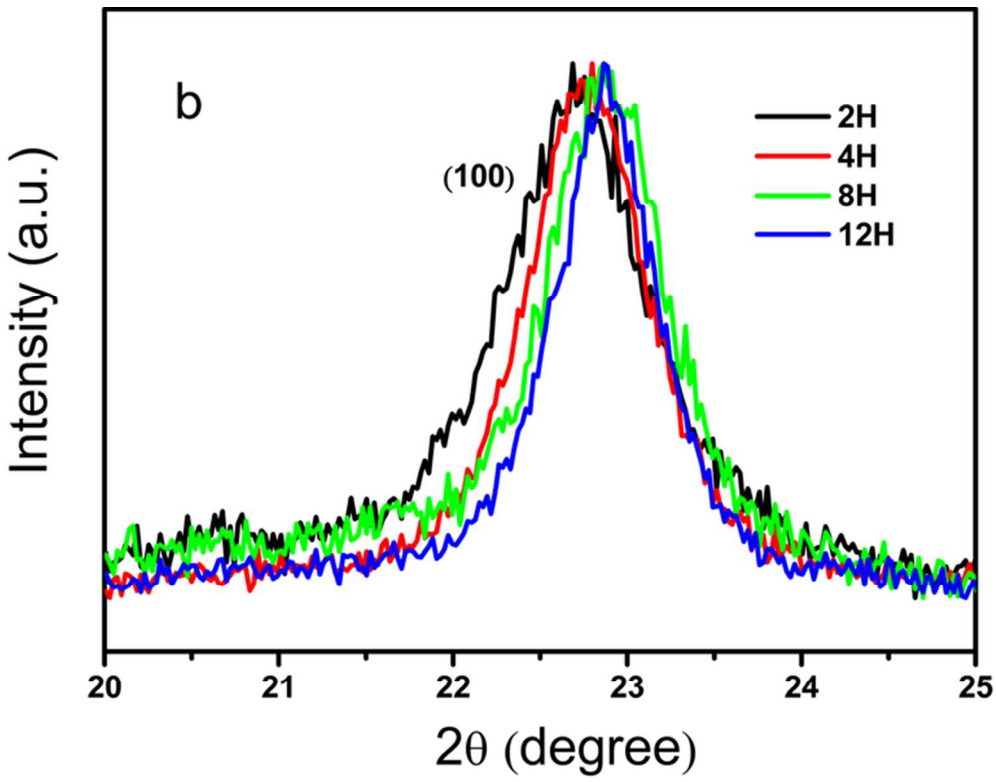

Figure 6. XRD pattern (a), enlarged (100) plane diffraction peak (b) of as-prepared NaTaO3 NPs with different reaction time.
65x50mm (300 x 300 DPI)

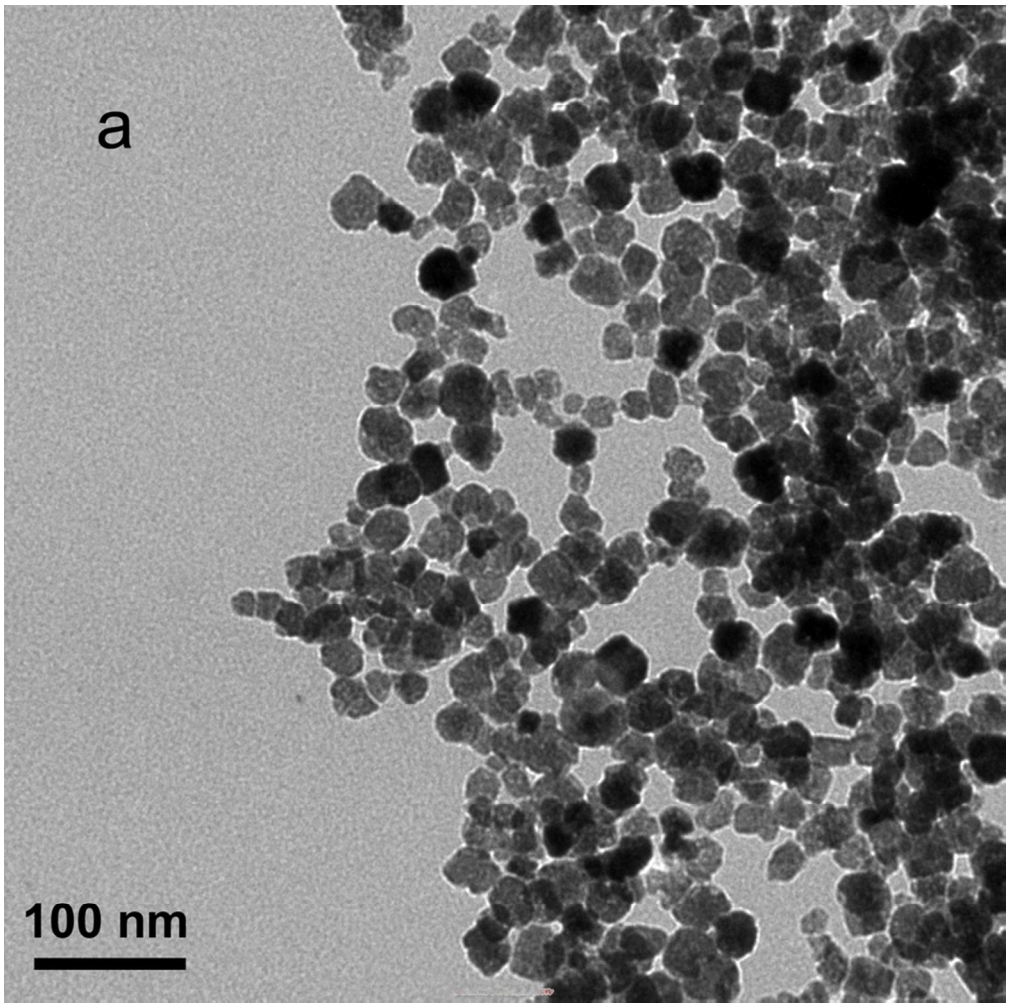

Figure 7. TEM images of NaTaO3 NPs prepared from Bicine (a), Triacetin (b), EDTA2Na (c).
84x84mm (300 x 300 DPI)

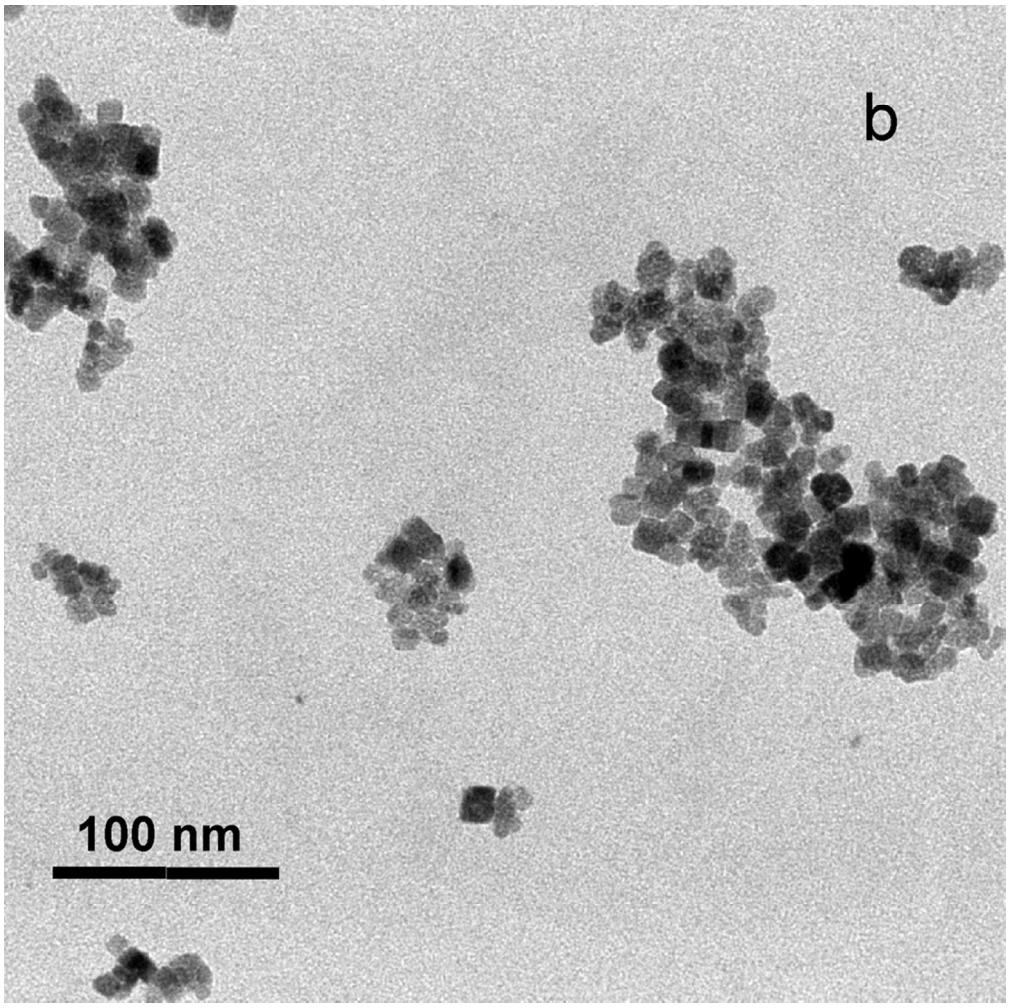

Figure 7. TEM images of NaTaO3 NPs prepared from Bicine (a), Triacetin (b), EDTA2Na (c).
84x84mm (300 x 300 DPI)

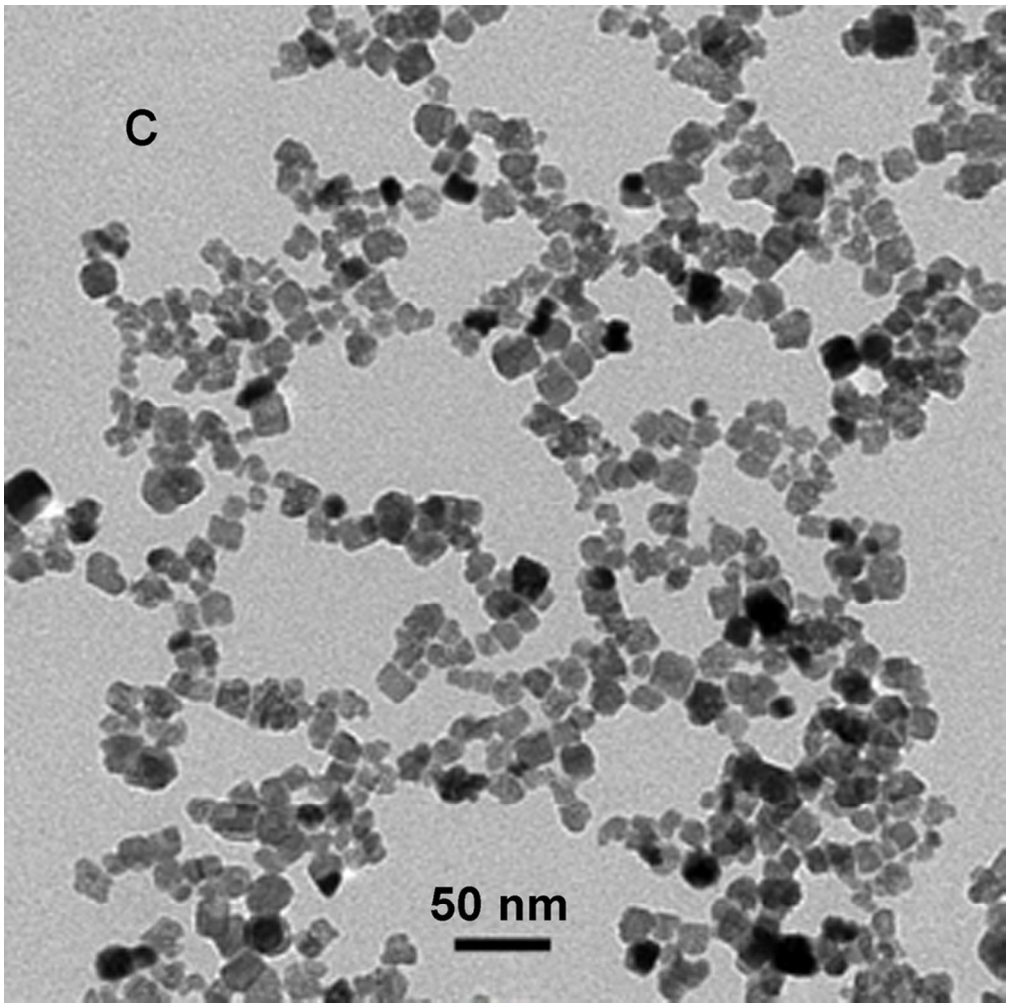

Figure 7. TEM images of NaTaO3 NPs prepared from Bicine (a), Triacetin (b), EDTA2Na (c).
84x84mm (300 x 300 DPI)

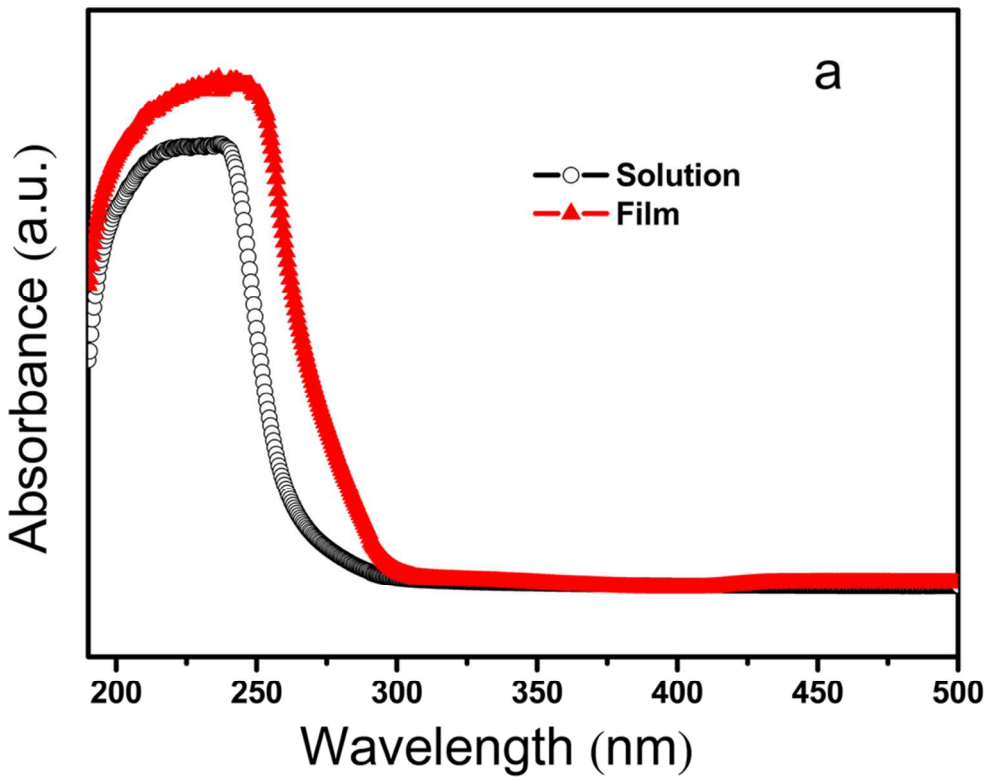

Figure 8. UV-vis absorption spectra of the NaTaO3 solution and spin-coating film (a), CV curve of the NaTaO3 spin-coating film (b).
85x65mm (300 x 300 DPI)

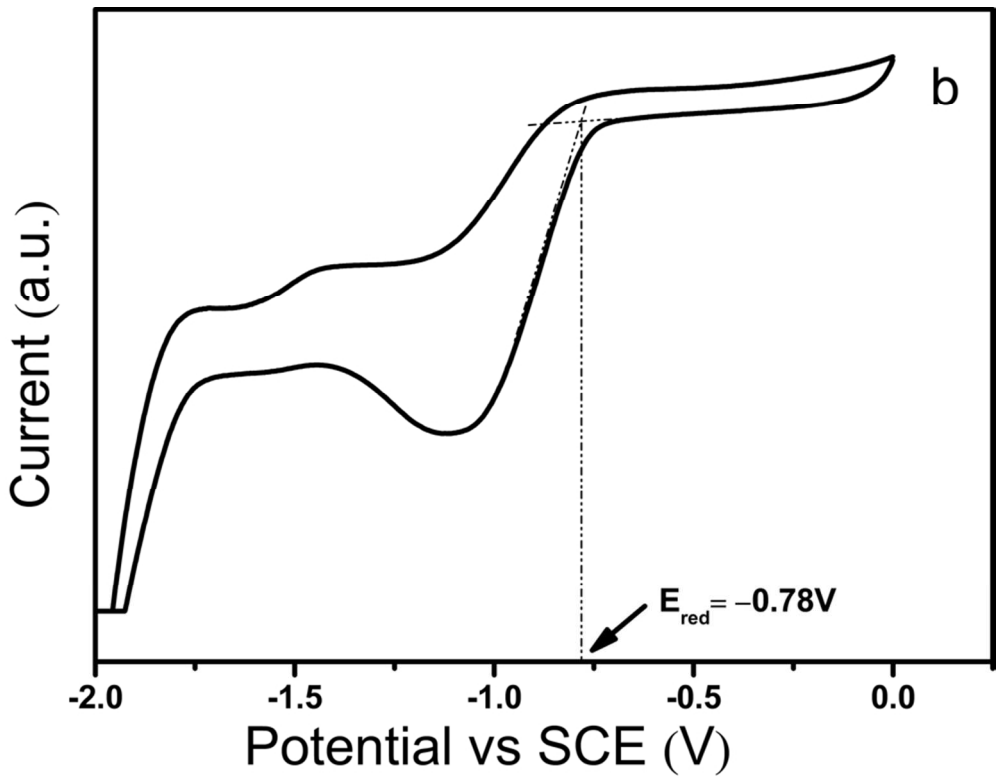

Figure 8. UV-vis absorption spectra of the NaTaO3 solution and spin-coating film (a), CV curve of the NaTaO3 spin-coating film (b).
85x65mm (300 x 300 DPI)

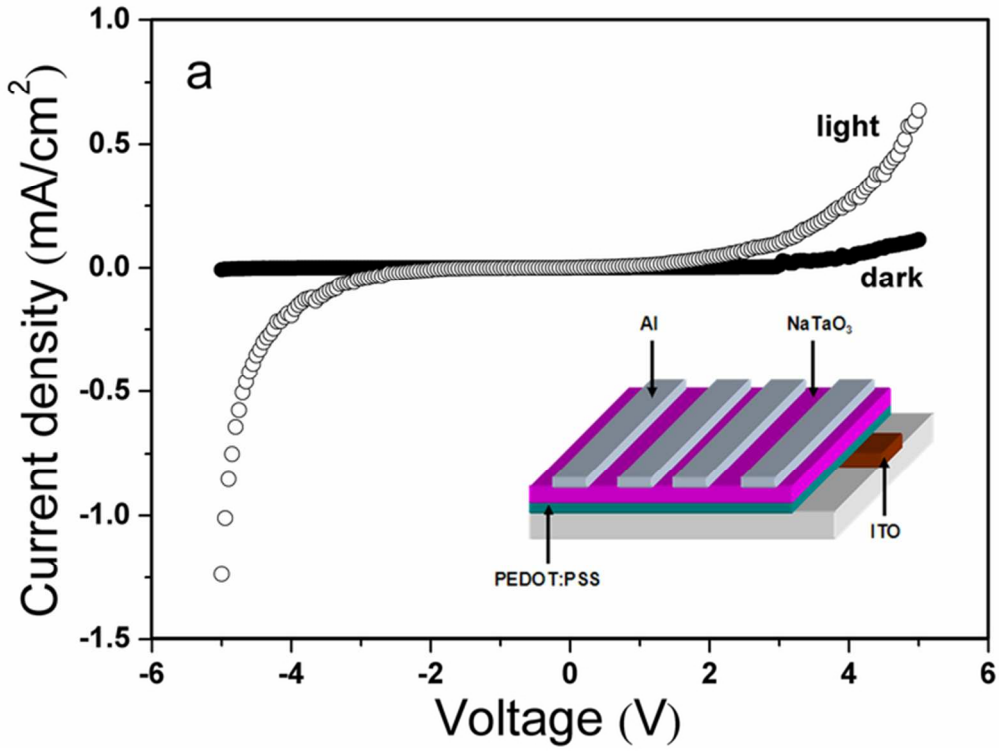

Figure 9. J-V curves in the dark and under 3.6mW/cm2 280 nm UV radiation (a), Transient response curve at -0.2V (b).
64x48mm (300 x 300 DPI)

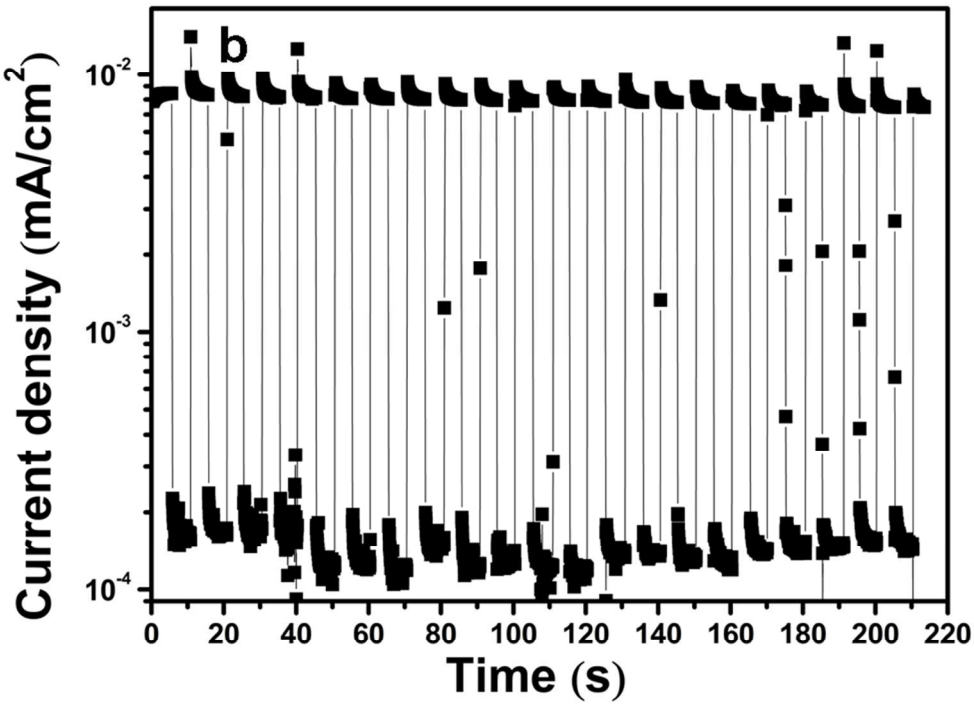

Figure 9. J-V curves in the dark and under 3.6mW/cm2 280 nm UV radiation (a), Transient response curve at -0.2V (b).
85x64mm (300 x 300 DPI)